Quantitative Trace Level Voltammetry in the Presence of Electrode Fouling Agents: Comparison of Single-Walled Carbon Nanotube Network Electrodes and Screen-Printed Carbon Electrodes

Sharel P. E, [‡,†] Thomas S. Miller, [‡,§] Lingcong Meng, [‡,¶] Patrick R. Unwin*[‡] and Julie V. Macpherson*[‡]

[†]School of Health & Life Sciences, Teesside University, Middlesbrough, TS1 3BX, UK

[‡]Department of Chemistry, University of Warwick, Coventry, CV4 7AL, UK

§Electrochemical Innovation Lab, Department of Chemical Engineering, University College London, Torrington Place, London WC1E 7JE, UK

[¶]School of Chemistry, University of Southampton, Southampton SO17 1BJ, UK

E-mail: j.macpherson@warwick.ac.uk, p.r.unwin@warwick.ac.uk; Fax: (+44) 02476 524112

Abstract

Single walled carbon nanotube (SWNT) network electrodes, in which a planar arrangement of SWNTs on an inert surface serves as a working electrode for voltammetry, offer considerable attributes for electroanalysis. Here, the effect of SWNT network density on the trace voltammetric analysis of a water-soluble ferrocene derivative (FcCOOH) is investigated in the presence of polyethylene glycol (PEG) or albumin, species that can foul (block) an electrode via adsorption. Fc-based analytes typically find use in redox labelling or redox shuttling, point of care electrochemical detection devices. Comparison is made between SWNT electrodes, grown by catalyzed chemical vapour deposition at three different surface coverages, 5, ~20 and ~30 $\mu m_{SWNT}\ \mu m^{-2}$, and commercial screen-printed carbon electrodes (SPCEs). In the presence of PEG (8% 2K), for cyclic voltammetry, the lowest detectable concentration decreases as SWNT network density decreases. However, when employing differential pulse voltammetry, all three networks show a 1 nM FcCOOH limit of detection, three orders of magnitude smaller than achievable with SPCEs. This is attributed to the low capacitance of the SWNTs and absence of amorphous carbon structures which can contribute a pseudo-capacitive response. For both polyethylene glycol (PEG) and albumin (4%), repeat cycling shows the higher density SWNT network electrodes ($\geq$ 20 $\mu m_{SWNT}\ \mu m^{-2}$) are far less susceptible to electrode fouling. Toward practical devices, a three-electrode chip, similar in design to that used in SPCEs, but using high density SWNT network electrodes, is also demonstrated to have impressive detection sensitivity for FcCOOH (nM level) in PEG solutions. The simplicity and practicality of the design widens the potential applications of these ultra-sensitive diagnostic tools based on planar network SWNTs.

Keywords: single walled carbon nanotubes, nanomolar detection, differential pulse voltammetry, albumin, polyethylene glycol, screen printed carbon electrode, electroanalysis, electrode fouling, blocking

Introduction

Interest in point-of-care (POC) detection is on the rise [1, 2], with many commercial devices using either optical or electrochemical (EC) based detection methods [1, 2]. In the EC arena, carbon-based sensors have become the subject of intense investigation especially for biomedical applications [3, 4]. Screen-printed carbon electrodes (SPCEs) are a popular choice for POC devices due to their reproducible manufacture in high volumes leading to low cost and disposability [5]. However, a limitation of SPCEs is that the commercial ink formulations, containing carbon particles, such as graphite, carbon black and activated carbon, and non-conducting binders such as polyvinylidene fluoride and polycarbonate, are usually unknown to the researcher (customer). The various ink components can affect the EC properties in different ways [6] and the background currents of such electrodes can be significant, containing both non-faradaic and pseudo-capacitive contributions, limiting detection limits in practical devices. Finally, the surface electrochemical properties are highly heterogeneous [7] and can vary from one electrode device to another [8].

Among carbon nanomaterials, single-walled carbon nanotubes (SWNTs) have attracted particular interest in EC analysis due to their promising physical and chemical properties, including chemical stability, biocompatibility, high sensitivity and low background currents [9]. However, the method of growth and preparation can also impact the resulting EC response. SWNTs grown by non-chemical vapour deposition (CVD) methods, e.g. electric arc discharge, typically contain appreciable levels of impurity catalytic nanoparticles and amorphous carbon that will contribute to the EC response, unless appropriately cleaned before use [9, 10]. SWNT electrodes prepared by dispersing the nanotubes onto a conducting electrode substrate by spin-coating, drop casting [9, 11, 12] or printing [13] can show interference in the EC response from the support material [9]. These methods can also result in high and uneven coverages of the

SWNTs, and large background currents [9, 14]. In contrast, the direct growth of SWNTs on insulating substrates using catalytic CVD provides electrodes with controllable surface coverage, spanning 1D, 2D and 3D arrangements [9]. Moreover, the resulting SWNTs have a low defect density [15], low amorphous carbon content and are relatively free of catalytic nanoparticles (NPs) [9], such that post-growth cleaning or treatments are not required.

The ability to control the growth density and SWNT arrangement is important as the non-faradaic, or background, current is an important issue for the practical sensitivity of amperometric/voltammetric sensors. The background current typically scales with electrode area [16]. A further issue to consider is possible electrode fouling during use, resulting in changes to the EC response, detection limit and the lifetime of an EC sensor. Previous work from our group showed that increasing SWNT surface coverage helped to mitigate electrode fouling effects due to the higher density of active electrode material and/or the lower mass transport per SWNT length [17, 18]. Thus, where fouling could be a problem, but a low-level of detection sensitivity is required, careful tailoring of SWNT coverage in an electrochemical (voltammetric) sensor is extremely important.

In many POC applications which employ EC detection, especially those requiring the analyte of interest to be redox labelled e.g. in DNA amplification and detection strategies [2, 19], iron based transition metals, such as ferrocene and its derivatives are often used [19-21]. This is due to the well-understood electrochemistry of this redox moiety *i.e.* fast electron transfer leading to diffusion-limited processes at moderate potentials, high stability and synthetic simplicity [22]. Detection is typically via either voltammetry [23, 24], or voltammetric amplification e.g. square wave or differential pulse voltammetry [19, 25]. In blood glucose POC devices, ferrocene / ferricyanide and related redox shuttles are also often employed [26]. In such systems, potential electrode fouling (blocking) agents include polyethylene glycol (PEG) and

albumin. PEG is a highly water-soluble and nontoxic polymer [27] and is often present as a component of one of the treatment solutions e.g. during amplification or enzymatic cleavage [28]. Whilst PEG is commonly used grafted to electrode surfaces to reduce non-specific protein adsorption [29], it can itself adsorb directly from solution, as has been reported for metal electrodes [30, 31]. Albumin is the most abundant protein found in blood plasma [32] and is known to adsorb to both carbon [33] and metal electrodes [34]. Adding albumin to an electrolyte solution provides a useful mimic of the blood environment [18]. The presence of both species also results in an increase in solution viscosity reducing EC detection signals due to the diminished diffusion coefficients.

In this paper, we examine the effect of SWNT surface coverage on the EC detection limit of a Fc-based moiety, here FcCOOH, in the presence of two electrode blocking agents first PEG and then albumin. The SWNTs are grown by catalysed CVD on an insulating substrate, as this process produces clean SWNTs, without the need for further processing, with controllable surface coverage [16] (*vide infra*). The results are compared against those obtained using commercial SPCEs. Finally, after identification of the most effective SWNT density for both low concentration detection and reduced fouling, we produce and demonstrate a user-friendly SWNT 3-electrode format for electroanalysis, akin to that found with SPCE platforms. Our SWNT device contains a SWNT working electrode and SWNT counter electrode on a single planar chip, onto which a quasi-silver reference electrode is evaporated.

Experimental

Chemicals and solutions

All chemicals were used as received. Aqueous solutions were prepared using deionized water produced by a Purite Select HP system (resistivity of 18.2 MΩ cm at 25 ^{o}C). FcCOOH (VWR

International Ltd., 98 %) was prepared in 8 % (weight/weight (*w/w*)) of PEG 2K (VWR International Ltd., UK) and 0.01 M phosphate-buffered solution (PBS, pH 7). PBS was prepared in-house from sodium phosphate dibasic heptahydrate ($Na_2HPO_4{\cdot}7H_2O$, Sigma-Aldrich, 98 – 100 %, UK) and sodium dihydrogen orthophosphate dihydrate ($NaH_2PO_4{\cdot}2H_2O$, Fisher Scientific, 99 – 100 %, UK). 4 % (*w/w*) albumin (Sigma-Aldrich, 97 %, UK) electrolyte was prepared in 0.01 M PBS.

Electrode materials

SPCE. Figure 1a shows a schematic of a 3-electrode SPCE (Kanichi Research, UK), consisting of a 3 mm diameter graphite disk as the working electrode (WE), a hemispherical band of graphite as the counter electrode (CE) and a quasi Ag/AgCl reference electrode (RE), printed onto polyvinyl chloride.

Controlled growth of SWNT Networks: SWNT networks were grown on 2 cm × 2 cm silicon (Si) substrates with 300 nm of thermally grown silicon oxide (SiO_2: IDB Technologies Ltd., n-type, 525 µm thick Si) using CVD. Iron nanoparticles (Fe NPs) were used as catalysts [35] for the growth of low density (LD) networks, whereas cobalt (Co) NPs were employed as catalysts [18] for both high density (HD) and super HD (SHD) networks. Fe NPs were deposited by soaking the Si/SiO_2 substrate in 1 % ferritin (50 – 150 mg mL^{-1}, Aldrich, UK) aqueous solution for 1 hour, followed by a 2 min exposure to a 100 W oxygen plasma (Emitech K1050X plasma asher, UK). Co was deposited by sputtering (SC7640 sputter coater, Quarum Techologies Ltd., UK) at 1 kV for 20 s and 30 s, respectively, for the growth of HD and SHD SWNT networks.

Patterned SHD SWNTs: A Kapton film mask compatible in size with a 1.7 cm × 2 cm Si/SiO_2 substrate, was prepared using laser micromaching (Oxford Lasers Ltd. E-355H-3-ATHI-O). The laser system was equipped with a Q-switched fully diode-pumped solid state Nd:YAG

laser medium with a primary output wavelength of 355 nm. Specifically, an area of 0.1 cm by 1.5 cm was exposed for the WE and 0.2 cm by 1.5 cm for the CE. Co NP catalyst deposition was carried out as described above and then the Kapton film mask was removed.

SWNT Growth: The Si/SiO_2 substrate was heated from room temperature to 850 ^oC over a period of 14 min under H_2 (BOC Gases, 99.95 %, UK) atmosphere at a flow rate of 150 sccm, followed by 1 min stabilization at 850 ^oC. The carbon feedstock, ethanol (Fisher, 99.99 %, UK) was then introduced via a flow of Ar (BOC Gases, 99.9995 % UK) (850 sccm) held at 0 ^oC. Growth was carried out for 10, 20 and 30 mins for low density (LD), high density (HD) and super high density (SHD) SWNT networks, respectively. The system was left to cool under H_2 gas. Electrical contact to the SWNT networks was achieved by evaporating a band, at one edge, of Cr (3 nm) followed by Au (60 nm). For the patterned electrode, Ag (60 nm) was evaporated through a shadow mask, using a Moorfields MiniLab deposition system (Moorfield Associates, UK), to form both a 0.1 × 1.5 cm quasi Ag RE and an electrical contact to the SWNT WE (0.1 cm × 0.6 cm) and CE (0.2 cm × 0.6 cm). Figures 1b and 1c respectively show the unpatterned and patterned SWNT network electrodes.

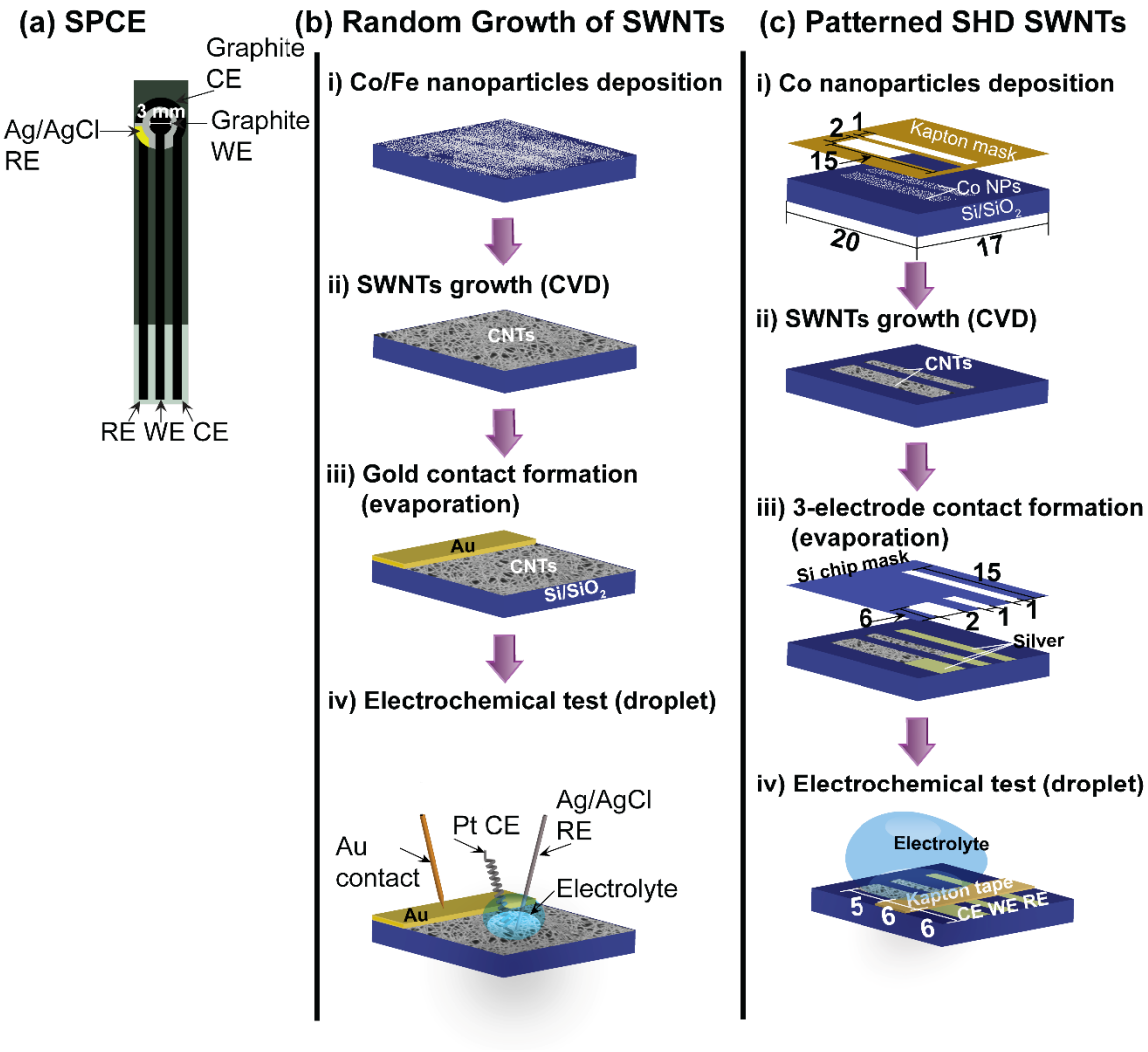

Figure 1: Schematic of the different 3-electrode arrangements employed: (a) SPCE. (b) Network SWNTs on an insulating surface produced by i) catalyst deposition, ii) SWNT CVD growth, iii) gold contact for the SWNT working electrode, iv) outlines the experimental arrangement for electrochemical measurements. (c) SWNT patterning processes to produce a SWNT electrochemical device on an Si/SiO_2 substrate showing i) catalyst NP deposition, ii) SWNT growth via CVD, iii) electrode contact and Ag quasi RE formation using evaporation and iv) the electrochemical droplet method. The unit of length for all numerical labels is mm.

SWNT network and SPCE characterization

Field emission scanning electron microscopy (FE-SEM) images were acquired (n = 3) using a Zeiss Supra 55-VP at 1 kV acceleration voltage to visualize the SWNT networks with different

densities and the microstructure of SPCEs. Micro-Raman spectra were recorded using a Renishaw inVia Raman microscope (514.5 nm Ar laser, 10 mW, $n = 3$).

Electrochemical experiments

To perform droplet measurements in the configuration of Figure 1b (iv), SWNT networks were connected as the WE. A drop of electrolyte solution (~15 µL, 4 mm diameter) containing FcCOOH mediator, 0.01 M PBS and either 4% albumin or 8% PEG 2K, was placed on the electrode surface, close to the Au band but without making contact with it. An AgCl-coated Ag wire acted as a quasi-RE and a platinum wire was used as a CE. Both were carefully positioned within the drop of solution to complete the 3-electrode arrangement. The electrochemically active area of the SWNT patterned electrode, was defined using kapton tape (1.7 cm × 0.6 cm), resulting in ca. 0.05 cm^2 area for the WE, 0.1 cm^2 for the CE and 0.05 cm^2 for the RE. A drop of solution containing redox mediator and supporting electrolyte was placed on the surface, so as to cover all 3 electrodes (Figure 1c (iv)). For all experiments, bar the fouling studies, a fresh area of the electrode surface was utilised for each different concentration of FcCOOH.

EC measurements were conducted using a CH Instruments (Austin, TX; model 1040A) potentiostat. CV and differential pulse voltammetry (DPV) were used for the EC measurements. DPV scans were recorded at 50 ms pulse width, 20 mV potential step, 200 ms pulse period with an potential amplitude of 50 mV. All EC measurements were carried out without a Faraday cage.

Results and discussion

SWNTs networks of controlled surface coverage

All SWNT networks in this study had a connectivity greater than the metallic percolation threshold ($\rho_{th(\text{metallic})}$, 1.4 – 2.4 $\mu m_{SWNT}\ \mu m^{-2}$; based on typical SWNTs lengths of 7 – 12 μm with sufficient metallic (m)SWNT to mSWNT connections to act as an electrode material.[17] cCVD growth typically results in 1/3rd of the SWNTs with metallic characteristics, the remaining 2/3rd are semiconducting (p-type) [36, 37]. Figure 2a shows a typical FE-SEM image of a LD SWNT network, which has a density of 5 (±1) $\mu m_{SWNT}\ \mu m^{-2}$. For HD and SHD SWNTs, it is difficult to accurately determine the network density using FE-SEM owing to the aggregation of individual SWNT to bundles. This is evidenced by the obvious layering of CNTs with the increase of SWNT density (Figure 2b and c). The surface morphology of a SPCE is illustrated in Figure 2d showing the significant heterogeneity of the surface.

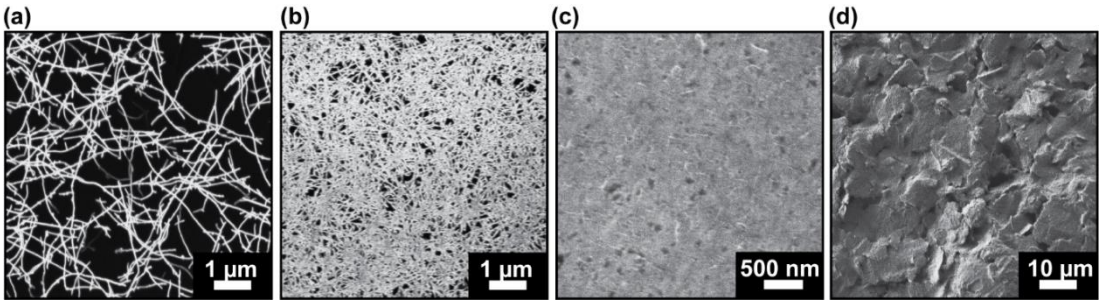

Figure 2: Typical FE-SEM images of (a) LD, (b) HD, (c) SHD SWNT networks, and (d) SPCE.

Due to the aggregation of SWNTs for the HD and SHD electrodes, the network density was instead estimated from the double layer capacitance, as the non-faradaic current would be reasonably expected to scale with the density of SWNTs. CVs (scan rate 100 mV s^{-1}) of the LD, HD and SHD SWNT network electrodes, and the SPCE in supporting electrode (0.01 M PBS) and 8% PEG 2K, are shown in Figure 3 and the calculated capacitance values are

summarized in Table 1. The specific capacitance values, C, of 60 ± 5 nF cm^{-2} (LD SWNT); 280 ± 15 nF cm^{-2} (HD SWNT); 400 ± 30 nF cm^{-2} (SHD SWNT) and 8600 ± 100 nF cm^{-2} (SPCE) were calculated from CVs presented in Figure 3, at 0 V versus Ag/AgCl, using:

$$C = \frac{i_{average}}{vA_{geometric}} \quad (1)$$

where $i_{average}$ is the average current magnitude of the forward and reverse sweep, v is the scan rate and $A_{geometric}$ is the geometrical area of the electrode. It is worth noting that the specific capacitances of the SWNT networks are ×20 (SHD), ×30 (HD) and ×140 (LD) lower than that of the SPCE. The HD SWNT network (Figure 2b) thus had an estimated density of ~20 μm_{SWNT} μm^{-2} calculated from the specific capacitance while the SHD SWNT network (Figure 2c) had an estimated density of ~30 μm_{SWNT} μm^{-2}.

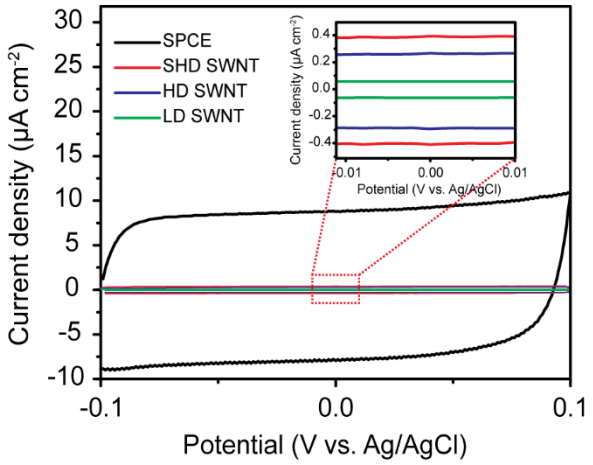

Figure 3: CVs for specific capacitance measurement in 8 % PEG 2K + 0.01 M PBS (100 mV s^{-1}) on SPCE (black), SHD (red), HD (blue) and LD (green) SWNT networks.

Figure 4 shows representative micro-Raman spectra of LD, HD, and SHD SWNT networks and SPCE, with the wavenumber ranging from 100 to 2600 cm^{-1}. For the SWNT networks, the peaks marked with (*) at 303 cm^{-1}, 521 cm^{-1} and 963 cm^{-1} originate from the Si/SiO_2 substrate and serve as a reference against which other peaks can be compared. In all spectra the presence

of the *G* peak (1585 cm^{-1}) indicates sp^2 carbon [38] and radial breathing modes[39] (RBM, 100 to 350 cm^{-1}) positively identify the networks as SWNTs. It is clear that the intensity of the *G* peak increases with the increased density of SWNTs in resonance with the Raman laser (*vide supra*).[39] The *D* peak at 1350 cm^{-1} originates from sp^3 carbon which can be found at defects or is due to amorphous carbon [40]. The intensity difference of the *G* peak to *D* peak is used as an indicator of the quality of SWNTs [41]. The *G* peak was *ca.* ×40, ×30 and ×20 the intensity of *D* peak for the LD, HD and SHD network SWNTs, respectively, confirming the high quality of the as-grown SWNTs, which have low intrinsic defect densities. In contrast, the *D* peak intensity of the SPCE is comparable with that of *G* peak which is possibly due to amorphous carbon and the binder that covers the SPCE surface [42]. Note, due to the resonance effect of the excitation energy and the absorption bands of SWNTs, the Raman count signal is much higher for SWNTs than for the SPCE [43].

Table 1 Estimated values of the network density from the specific capacitance of SWNT network electrodes and comparison to SPCE

Electrode	Specific capacitance (μF cm^{-2})	SWNT density estimated from specific capacitance (μm_{SWNT} μm^{-2})
LD SWNT	0.6 ± 0.005	5 ± 1 (determined from FE-SEM presented in Figure 2a)
HD SWNT	2.800 ± 0.015	~ 20
SHD SWNT	4.000 ± 0.030	~ 30
SPCE	86.000 ± 0.100	Not applicable

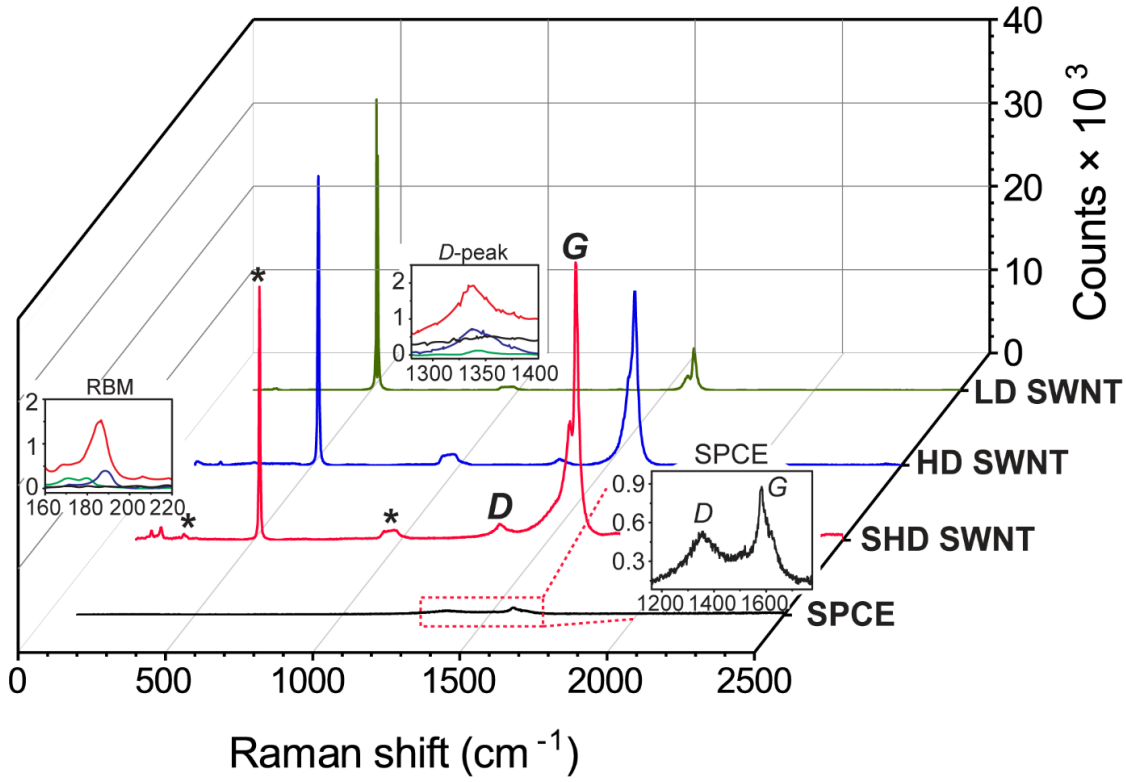

Figure 4 Micro-Raman spectra of SPCE (black), SHD (red), HD (blue) and LD (green) SWNT networks.

CV response and detection limit of FcCOOH for LD, HD, SHD SWNT network electrodes compared to SPCEs

CV was initially employed to analyze the detection sensitivity of FcCOOH oxidation at the three different SWNT network density electrodes and SPCEs, in a PEG-containing solution. The increased viscosity of the 8% PEG 2K solution results in a decrease of the diffusion coefficient for FcCOOH from 5.20×10^{-6} cm^2 s^{-1} to 3.50×10^{-6} cm^2 s^{-1}, supporting information, S1. Figure 5 shows typical CVs recorded over the FcCOOH concentrations range 15 nM – 100 µM in 8 % PEG 2K (*w/w*) and 0.01 M PBS, at a scan rate of 100 mV s^{-1}. Note that the current density is calculated based on the geometric area of each electrode device. The CVs in Figure 5a recorded on a LD SWNT network show a linear dependence of peak current (i_p) on

concentrations in the range 15 to 100 nM (inset) for the oxidation of FcCOOH. Even at 25 nM FcCOOH the oxidative current signal is easily discernible. The ability to distinguish such low concentrations voltammetrically, using the LD SWNT network is attributed to the very low intrinsic background current. This results from the significantly low density of SWNTs, as seen previously for solutions that did not contain possible adsorbing additives [16].

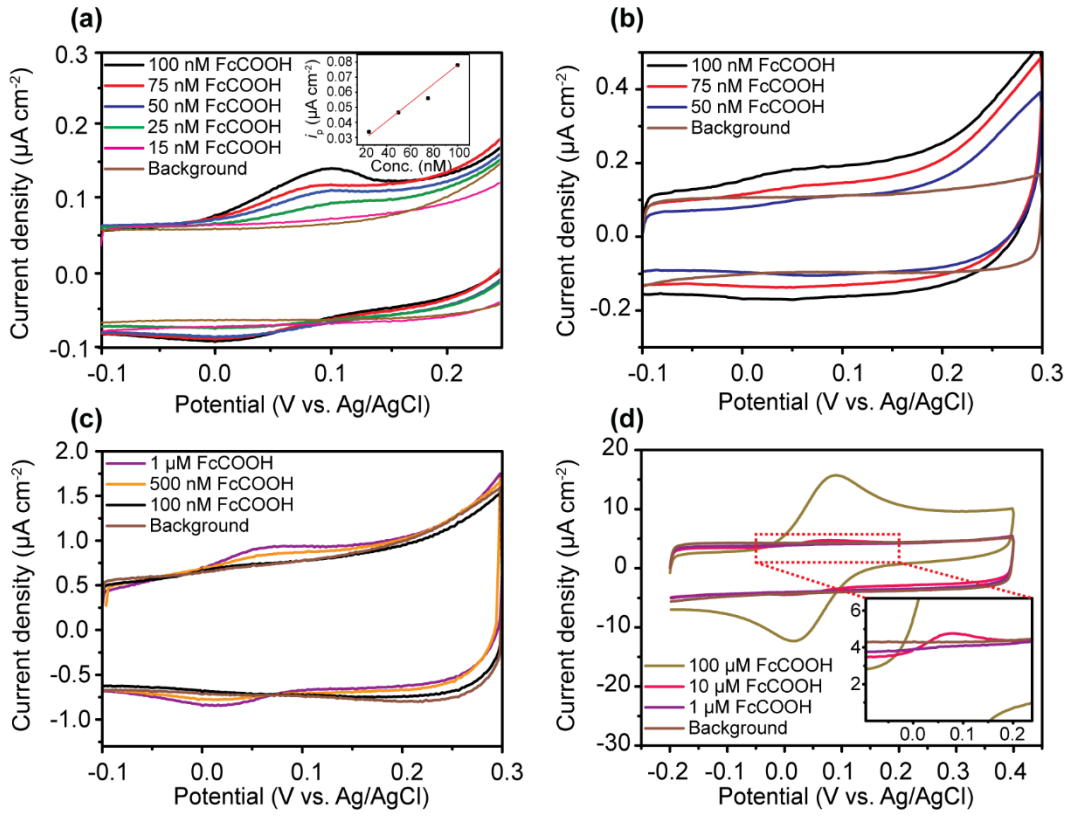

Figure 5 CVs for the oxidation of different concentrations of FcCOOH in 8% PEG 2K and 0.01 M PBS (100 mV s^{-1}) at (a) LD (Inset is the plot of i_p *vs.* Concentration), (b) HD, (c) SHD SWNT networks and (d) SPCE.

At the HD SWNT network electrode, a detectable redox current is observed for concentrations ≥75 nM FcCOOH (Figure 5b), while for the SHD SWNT network electrode, this value is ≥ 500 nM (Figure 5c). This behaviour is expected, as the capacitive background current scales with the SWNT network density which impairs the detection limit. Further capacitive

constraint was observed at SPCEs with a detectable concentration value which is significantly higher, ≥10 µM FcCOOH (Figure 5d).

The peak to peak separation (ΔE_p) for FcCOOH on the different electrodes was 62 mV (100 nM; HD SWNT), 60 mV (1 µM; SHD SWNT) and 72 mV (100 µM; SPCE), values which are reasonably close to reversible behaviour. This indicates facile ET kinetics for this one-electron oxidation, noting that the droplet arrangement is more prone to ohmic effects [44], which could influence the data with 100 µM and higher FcCOOH concentration. However, ΔE_p for the LD SWNT network at 100 nM FcCOOH is 90 mV. The larger ΔE_p value could be due to this network having the highest intrinsic resistance of all three networks, although we note that very small currents are passed. More likely, the apparent reduction in electrochemical kinetics is due to the LD network having a greater susceptibility to blocking effects (adsorption of PEG molecules to the surface), *vide infra*. Here the interplay between the electrochemical kinetics and the (already high) local diffusional flux at sparse SWNTs [45] will be pushed towards increasing apparent kinetic constraint by any further passivation of the SWNT surface.

DPV response of LD, HD, SHD SWNT network electrodes and SPCE

DPV was employed as a means of improving the detection sensitivity [46], focusing on the oxidation of FcCOOH in 8% PEG 2K solutions. As shown in Figure 6, the lowest detectable concentration was greatly improved for all electrodes, with concentrations of 5 nM for the LD SWNT (Figure 6a), 5 nM for the HD SWNT (Figure 6b), 1 nM for SHD SWNT (Figure 6c) now resolvable. The resulting peak current versus concentration plots were linear for all four electrodes, resulting in limits of detection (LOD) of 1.30 ± 0.01 nM (LD), 1.05 ± 0.04 nM (HD), 1.00 ± 0.003 nM (SHD) and 2.05 ± 0.06 µM (SPCE), for n = 4, Supporting Information S2. This result is very interesting in that it shows that for the SWNT networks, irrespective of

density, a similar LOD results, at the 1 nM level, when a potential pulse sequence is used to collect the data. Moreover, all three SWNT electrodes give a quantitative response to a concentration of FcCOOH that is *ca.* 1000 times lower than that obtained from the SPCE.

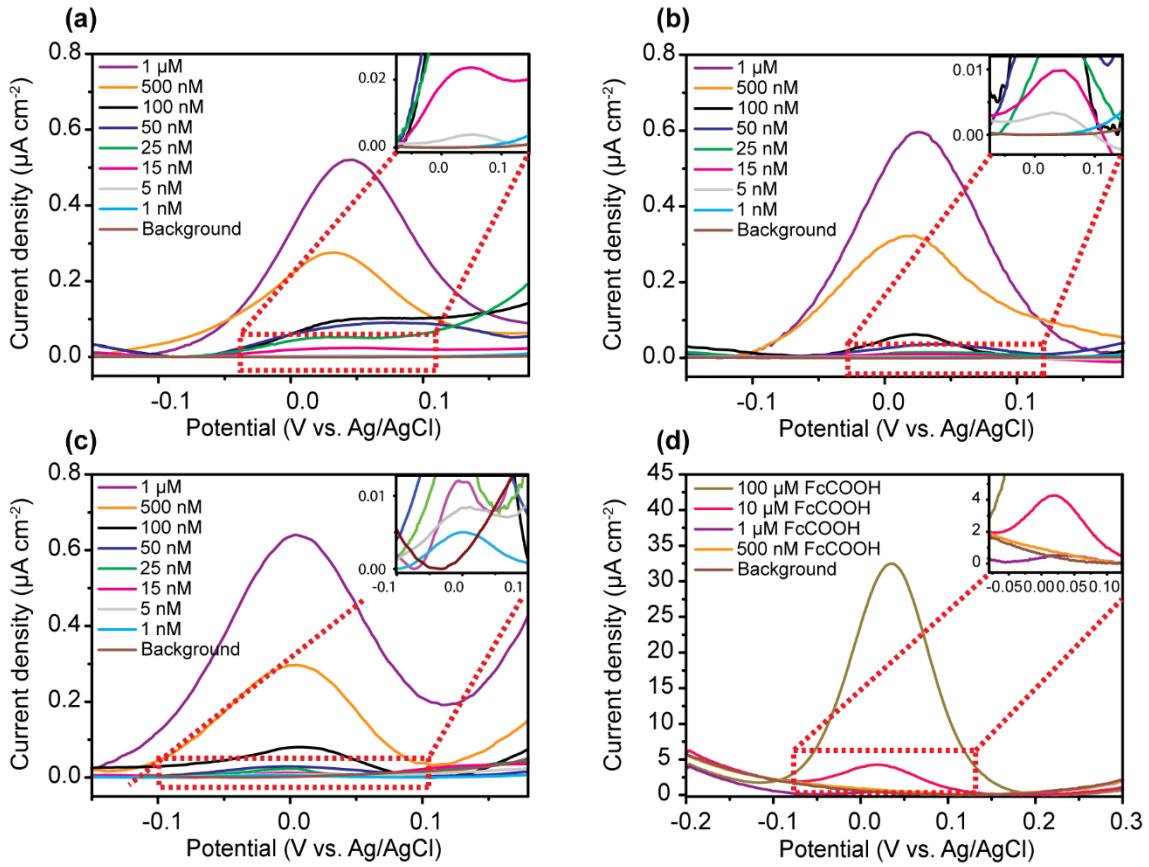

Figure 6 DPVs for the oxidation of different concentrations of FcCOOH in 8% PEG 2K and 0.01 M PBS at (a) LD, (b) HD, (c) SHD SWNT networks and (d) SPCE. Inset is a zoom-in to a particular region of the DPVs.

DPV, and other potential pulse techniques such as square wave voltammetry, decrease the detectable concentration by collecting currents in a region of the current-time curve (for each potential pulse) where the non-faradaic current has decayed to zero [47]. Under ideal conditions, the non-faradaic response will be controlled only by uncompensated resistance and double layer capacitance effects (RC). If the system suffers from high R or C contributions already, it may be difficult to sample the current under conditions where the non-faradaic

contribution has decreased to zero, due to the high time constant. Moreover, if pseudo-capacitive contributions are present, e.g. due to the presence of redox active molecules on the surface, such as quinone groups, an additional faradaic contribution will arise which cannot be negated using potential pulse techniques [47].

The results observed indicate that the RC component in the SWNT electrode system is small, even when the C is larger for the higher density electrodes. The cleanliness, low defect density and minimal levels of amorphous carbon of SWNTs grown by CVD, results not only in low values for the double layer capacitance per length of SWNT [48], but means there are unlikely to be any redox active groups on the SWNT surface. In contrast, the SPCE, which possesses by far the highest capacitive current, did not yield a particularly low detection limit (μM range) due to the complexity of the graphitic surface, composed of organic oil, binder paste and the presence of other surface redox groups (such as surface-bound quinones) [6, 49].

Fouling Effects of Additives

To investigate the fouling effect of additives on the SWNT networks electrodes and the SPCE, either 8% PEG 2K [50] or 4% albumin [18] was added to the analyte solution [33, 51] and the CV cycled a sufficient number of times in order to observe noticeable trends in the peak current. Here we used fifteen cycles. Given the high background currents of the SPCE electrode (Figure 5d), in order to observe a clearly distinguishable peak current, a concentration of 100 μM FcCOOH was used for all electrodes. Figure 7 shows fourteen repeat cycling CVs (starting from the second CV) for FcCOOH oxidation in 8% PEG 2K on SWNT networks of LD (Figure 7a), HD (Figure 7b), SHD (Figure 7c) and SPCE (Figure 7d). As the CVs were cycled continuously, and no wait time implemented, we show only the CVs starting from the second scan due to the possible contribution of analyte depletion effects which will be felt most

severely from the first to second scan (first CV cycle for each run is in Supporting Information, S3).

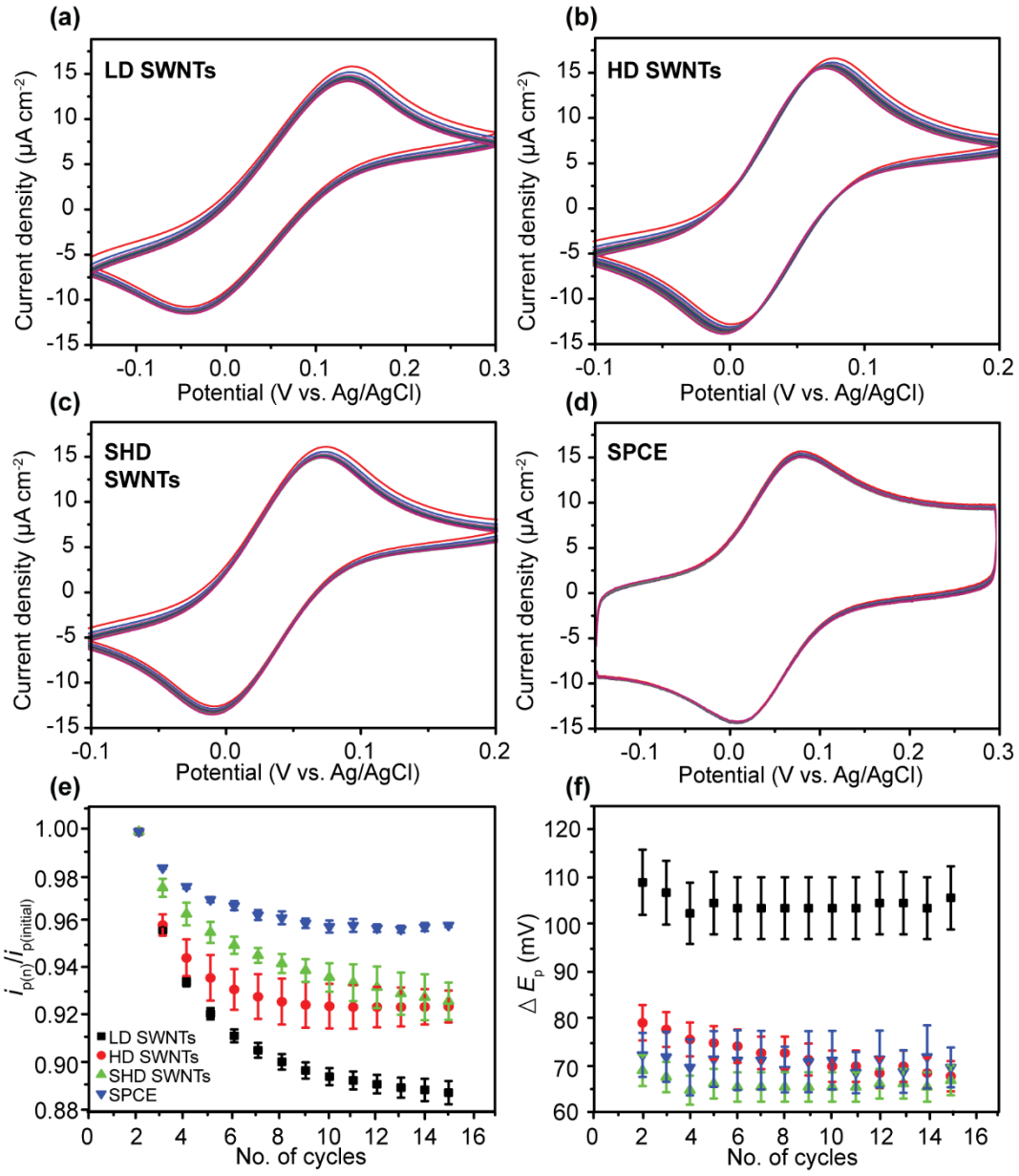

Figure 7: CVs of 14 consecutive cycle from the second scan for the oxidation of 100 μM FcCOOH in 8 % PEG 2K and 0.01 M PBS at (a) LD, (b) HD, (c) SHD SWNT networks and (d) SPCE, scan rate 100 mV s^{-1}. (e) $i_{p(n)}/i_{p(initial)}$ versus number of scan cycles (f) ΔE_p versus number of scan cycles. (n = 3).

Figure 7e shows summary data of i_p normalised by the value on the second scan as a function of number of CV cycles. i_p typically decreases with consecutive scans, with the extent depending on SWNT coverage and type of carbon electrode. It is obvious from Fig. 7a that the LD SWNT networks appear to be more susceptible to fouling than the other electrodes, with a drop in the FcCOOH oxidative peak current, i_p by 11.15 ± 0.5 % after fourteen CVs compared to an i_p drop of 7.5 ± 0.7 % for HD SWNTs (Fig. 7b), 7.1 ± 0.7 % SHD SWNTs (Fig. 7c) and 4.0 ± 0.2 % for SPCE (Fig. 7d). Figure 7f shows the summary data of ΔE_p as a function of number of CV cycles. For all electrodes, bar the LD SWNT network electrode, the change in ΔE_p is less than 10 mV over the fourteen cycles. For the higher density SWNT networks, the apparent faster electrochemical kinetics (smaller ΔE_p) and smaller observed decreases in i_p with increasing scan number, is attributed to the higher surface coverage of SWNTs. With a high density of active material, and contrary to the discussion on the LD SWNT network above, changes to FcCOOH mass transport per unit area of SWNT, as a result of SWNT blocking, will be less strongly felt. This is due to the rate of redox-reaction per unit area of active electrode material being much lower.

The effect of albumin in solution was investigated in a similar fashion using 100 μM FcCOOH and 4 % albumin (*w/w*), with CV data shown in Figure 8. Again, the response of the LD SWNT network shows greater susceptibility to fouling than the other electrodes, as judged by the diminution in CV response. In particular, the fifteenth scan data shows a drop in i_p of 16.0 ± 1.2 % (LD SWNT network, Figure 8a), compared to 2.0 ± 1.3 % (HD SWNT network; Figure 8b), 0.5 ± 0.2 % (SHD SWNT network; Figure 8c) and 13.0 ± 2.0 % (SPCE; Figure 8d).

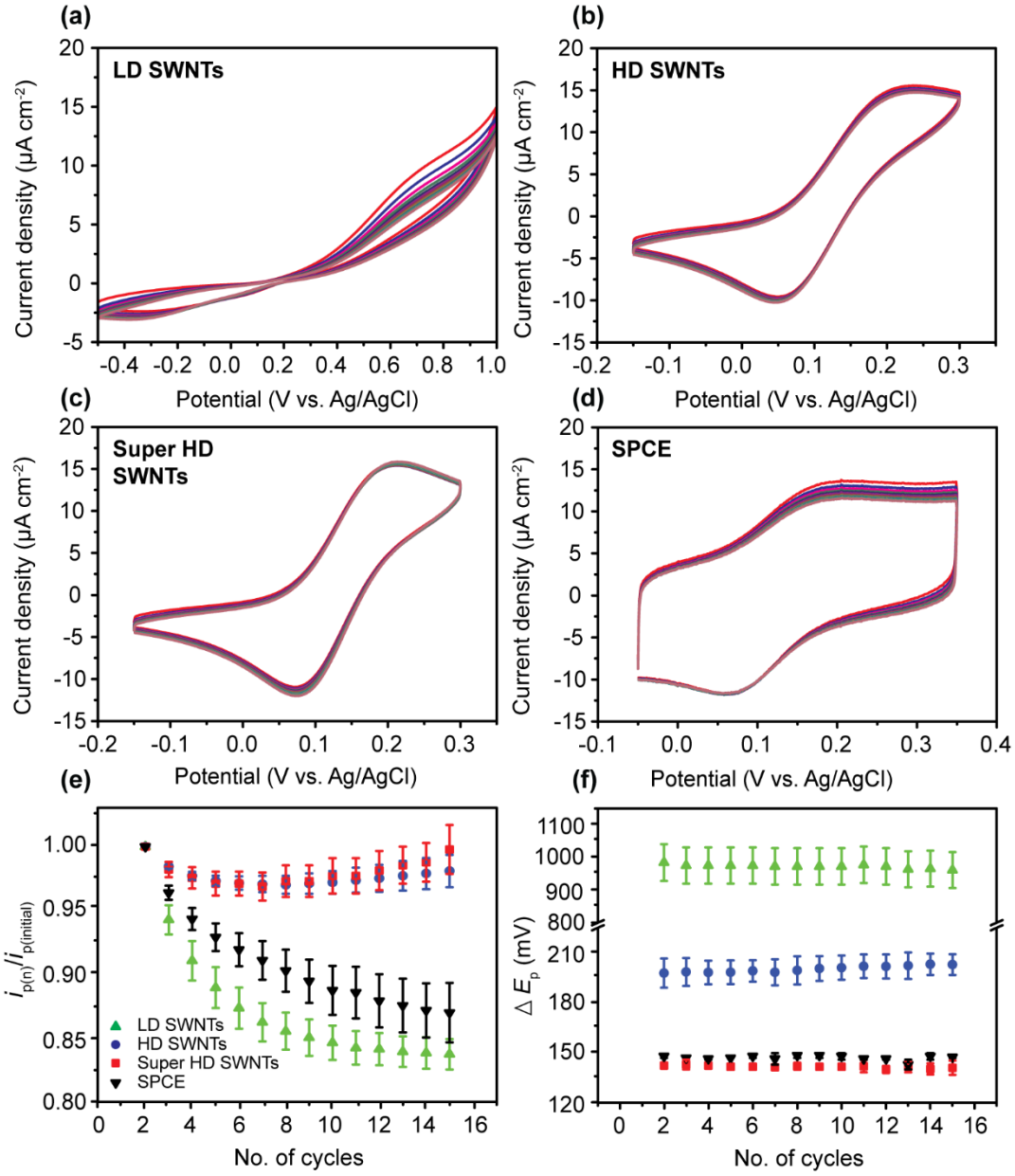

Figure 8. CVs of 14 consecutive cycles for the oxidation of 100 μM FcCOOH in 4 % albumin and 0.01 M PBS at (a) LD, (b) HD, (c) SHD SWNT networks and (d) SPCE, scan rate 100 mV s^{-1}. (e) $i_{p(n)}/i_{p(initial)}$ versus number of cycles (with the initial value taken from the second cycle – see text) and (f) ΔE_p versus number of cycles: SPCE (black), SHD SWNTs (red), HD SWNTs (blue), and LD SWNT networks(green). (n = 3).

The redox behaviour of FcCOOH for the different electrodes shows an average ΔE_p value (second to fifteenth cycle) of 140 ± 5 mV (SHD SWNT network), 200 ± 10 mV (HD SWNT network), 960 ± 50 mV (LD SWNT network), and 140 ± 5 mV (SPCE). Note the signicantly

increased ΔE_p for the LD SWNT network. In general, for all electrodes, the increased ΔE_p in 4% albumin compared to that in 8% PEG 2K, indicates apparently slower kinetics, attributed to stronger adsorption of albumin on the electrode surfaces.

Controllable preparation of a high density SWNT three-electrode cell

Based on the data above, both HD and SHD SWNT networks show promise as electroanalytical detectors in the presence of species that foul the electrode by adsorption. To this end, SWNT devices with a format similar to that of the SPCE, i.e. with WE, RE and CE tracks all on the same insulating substrate (chip) were prepared and tested electrochemically. A HD SWNT network (~20 μm length of SWNT per μm^{-2}) was used for these studies.

The photograph in Figure 9a shows the 3-electrode design, with the lithographically-defined HD SWNT network electrodes for the WE and CE, and a quasi-Ag electrode for the RE. Figure 9b shows a typical FE-SEM image of the 1 mm width HD SWNT network band on the inert Si/SiO_2 substrate, whilst Figure 9c is a higher resolution FE-SEM of the multiply-interconnected and randomly oriented SWNT networks. Figure 9d shows representative micro-Raman spectra of the HD SWNT network ranging from 100 to 2500 cm^{-1}. The *G* peak was *ca.* 30× the intensity of the *D* peak for HD SWNT network, indicating that the as-grown HD SWNTs have low intrinsic defect densities, matching well with the data in Figure 4.

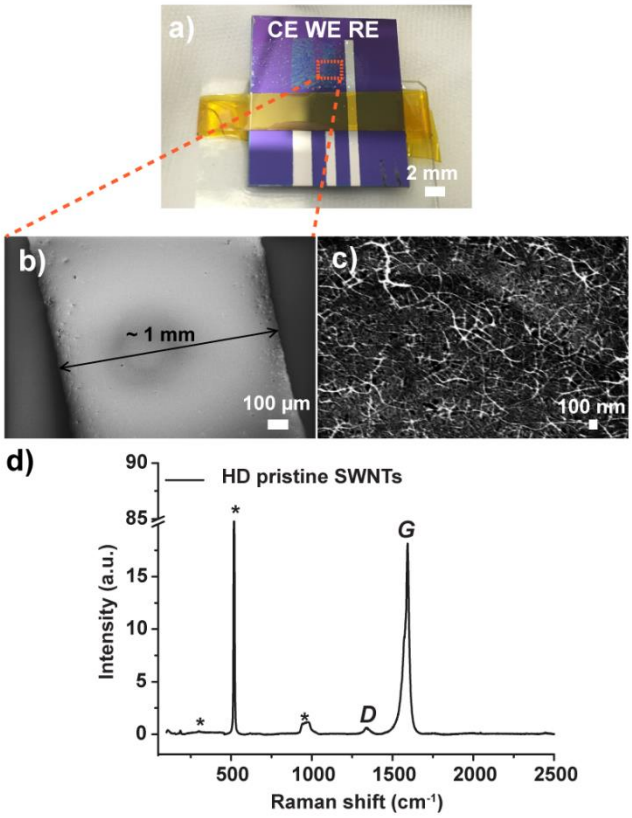

Figure 9 (a) Photograph of the 3-electrode SWNT patterned device. (b) FE-SEM image of 1 mm width SWNT network grown on the inert substrate acting as WE; (c) zoom of SWNT network. (d) Micro-Raman spectrum of SWNTs in the device.

Electrochemical characterisation of three-electrode SWNT chip using DPV

To demonstrate the electrochemical viability of the 3-electrode SWNT chip, a small volume of analyte solution (5 µL) was placed on the device and DPV employed for electroanalysis. Figure 10a shows typical DPVs recorded at different concentrations of FcCOOH, 25 nM (red), 50 nM (blue), 100 nM (magenta), 500 nM (olive), 1 µM (navy), and 5 µM (violet), in 8% PEG 2K (*w/w*) and 0.01 M PBS (black), $n = 3$. The response of 25 nM (red) is easily visible at the SHD SWNT network electrode (Figure 10b). Figures 10c and d show the plot of peak currents as a function of FcCOOH concentrations (25 nM to 5 µM) in 8% PEG 2K and 0.01 M PBS. The peak current increased linearly with FcCOOH concentration, with a gradient of 0.33 ± 0.01 A

cm^{-2} M^{-1} (R^2 = 0.99468) and a detection limit of 6.6 ± 0.2 nM for HD SWNTs. This data is in fairly good agreement with the lowest detectable concentration shown for the HD network operating in a droplet cell configuration, Figure 6b.

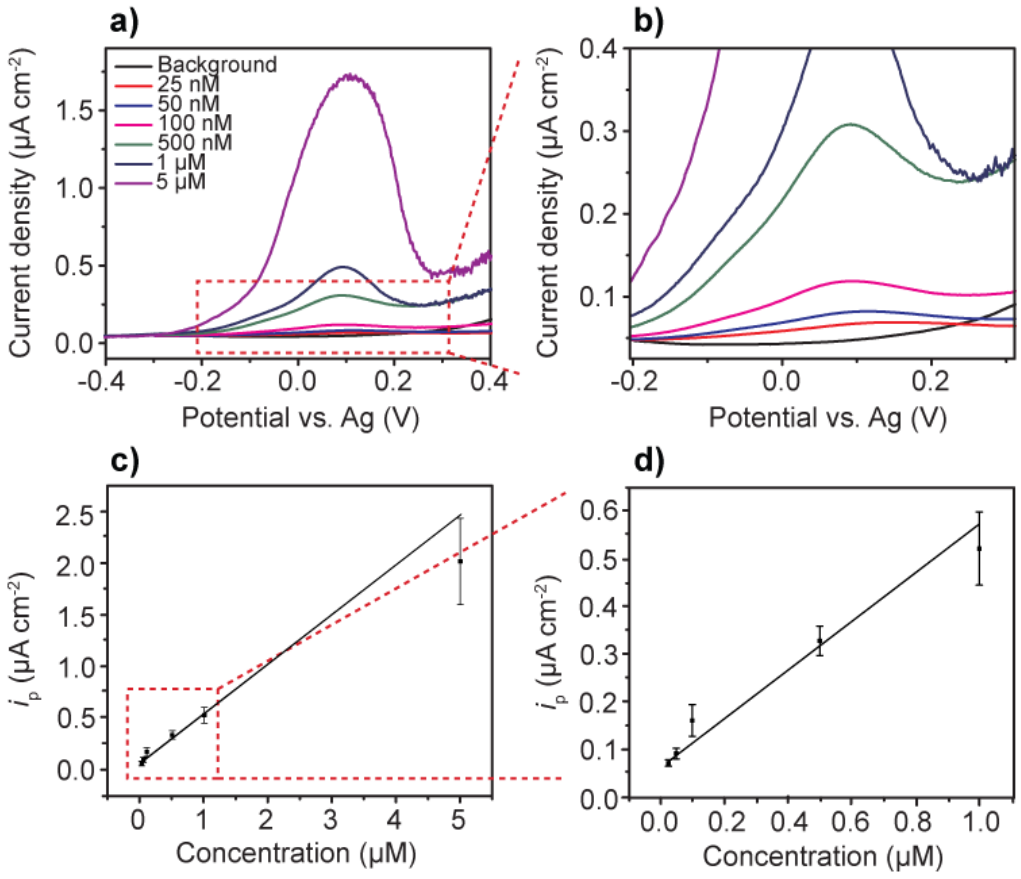

Figure 10. Electrochemistry at a HD SWNT 3-electrode chip. (a) Typical DPVs for the oxidation of different concentrations of FcCOOH (25 nM to 5 µM) in 8% PEG 2K and 0.01 M PBS. (b) Zoom of DPV curves to highlight the response of the lowest FcCOOH concentrations. (c) Plot of i_p (background corrected) versus concentration of FcCOOH and (d) magnification of the low concentration range (n = 3).

Conclusions

SWNT network electrodes have been demonstrated to be very effective for trace level FcCOOH voltammetric measurements in complex media containing the electrode fouling

agents PEG or albumin, which can adsorb to the electrode surface. SWNT network electrodes outperform SPCEs in terms of lowest detectable concentration, by up to three orders of magnitude. Using CV, in 8% PEG 2K solutions, the lowest detectable concentration for FcCOOH decreased as the network density decreased. Interestingly, with DPV, which removes non-faradaic contributions, the lowest detectable concentration was found to be relatively independent of network density, with all networks giving a FcCOOH detection limit of 1 nM, three orders of magnitude lower than achievable with SPCEs. This was attributed to the cleanliness of the SWNTs grown via CVD, resulting in low capacitive currents and absence of amorphous carbon which can contribute a pseudo-capacitive (faradaic) response.

Repeat cycling (fifteen cycles in total) of the three different density SWNT network electrodes in FcCOOH solutions containing either 8% PEG 2K or 4% albumin, showed that the LD networks suffered the most from fouling (adsorption) effects, impairing the electrochemical response and detection sensitivity. For LD SWNTs, the local high mass transport (flux) is very high, placing greater apparent kinetic demands on the active part of the electrode, and hence a greater sensitivity of the response to blocking. Such effects are much less significant for higher coverage SWNT devices; both the HD and SHD networks showed minimal fouling effects in 4 % albumin.

Finally, a lithographic patterning procedure was used to produce HD SWNT-based electrode devices (chips) which mimic that of the commercial SPCE. Such devices showed a detection limit for FcCOOH of 6.6 nM in the presence of 8% PEG 2K. The SWNT network electrode platform paves the way for trace voltammetric measurements at carbon electrodes, in a ready-to-use format. Compared to SPCEs, this device offers greatly improved sensitivity and detection limits in the presence of additives which can adsorb and block the electrode surface.

Acknowledgements

The authors thank Dr. Yang-Rae Kim, Dr. Aleix G. Güell, and Dr. Ashley Page for their help and support. SPE thanks the University of Warwick for the funding through the award of Chancellor's International Scholarship. TSM acknowledges support from EPSRC for a PhD studentship. The Royal Society is acknowledged for a Wolfson Research Merit Award to PRU and an Industry Fellowship to JVM.

Insert Table of Contents Graphic and Synopsis Here

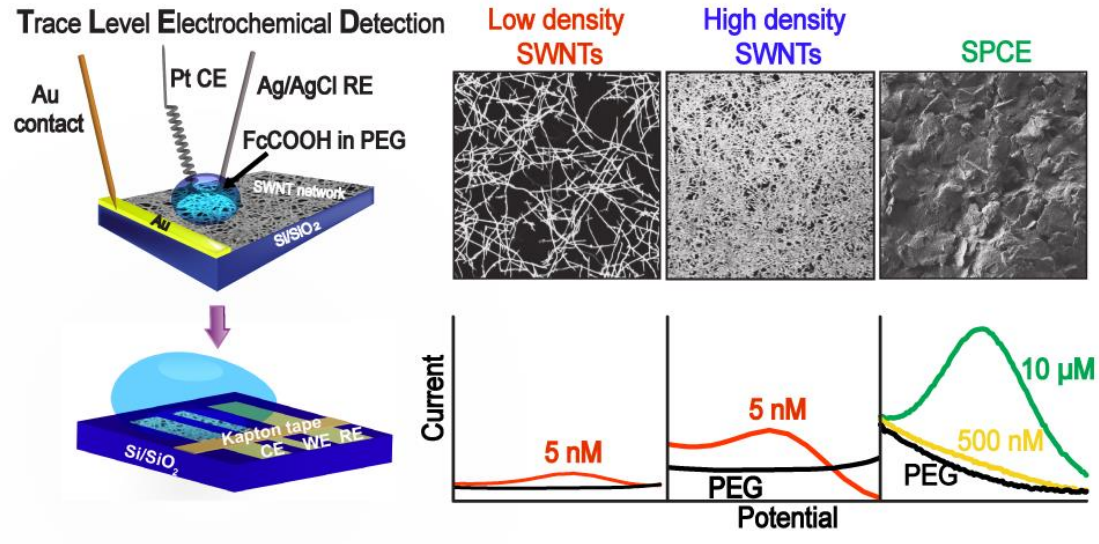

Comparison of single-walled carbon nanotube network and commercially available screen-printed carbon electrode for trace level electrochemical detection in biological media.

References

[1] D.C. Christodouleas, B. Kaur, P. Chorti, From point-of-care testing to eHealth diagnostic devices (eDiagnostics), ACS Cent. Sci., 4 (2018) 1600-1616. https://doi.org/10.1021/acscentsci.8b00625.

[2] V. Gubala, L.F. Harris, A.J. Ricco, M.X. Tan, D.E. Williams, Point of care diagnostics: status and future, Anal. Chem., 84 (2012) 487-515. https://doi.org/10.1021/ac2030199.

[3] C.B. Jacobs, M.J. Peairs, B.J. Venton, Review: Carbon nanotube based electrochemical sensors for biomolecules, Anal. Chim. Acta, 662 (2010) 105-127. https://doi.org/10.1016/j.aca.2010.01.009.

[4] J.N. Tiwari, V. Vij, K.C. Kemp, K.S. Kim, Engineered carbon-nanomaterial-based electrochemical sensors for biomolecules, ACS Nano, 10 (2016) 46-80. https://doi.org/10.1021/acsnano.5b05690.

[5] R.A.S. Couto, J.L.F.C. Lima, M.B. Quinaz, Recent developments, characteristics and potential applications of screen-printed electrodes in pharmaceutical and biological analysis, Talanta, 146 (2016) 801-814. https://doi.org/10.1016/j.talanta.2015.06.011.

[6] J. Wang, B.M. Tian, V.B. Nascimento, L. Angnes, Performance of screen-printed carbon electrodes fabricated from different carbon inks, Electrochim. Acta, 43 (1998) 3459-3465. https://doi.org/10.1016/S0013-4686(98)00092-9.

[7] D. Martin-Yerga, A. Costa-Garcia, P.R. Unwin, Correlative voltammetric microscopy: structure-activity relationships in the microscopic electrochemical behavior of screen printed carbon electrodes, ACS Sensors, 4 (2019) 2173-2180. https://doi.org/10.1021/acssensors.9b01021.

[8] F. Ghamouss, S. Ledru, N. Ruillé, F. Lantier, M. Boujtita, Bulk-modified modified screen-printing carbon electrodes with both lactate oxidase (LOD) and horseradish peroxide (HRP) for the determination of L-lactate in flow injection analysis mode, Anal. Chim. Acta, 570 (2006) 158-164. https://doi.org/10.1016/j.aca.2006.04.022.

[9] I. Dumitrescu, P.R. Unwin, J.V. Macpherson, Electrochemistry at carbon nanotubes: perspective and issues, Chem. Commun., 45 (2009) 6886-6901. https://doi.org/10.1039/B909734A.

[10] C.E. Banks, A. Crossley, C. Salter, S.J. Wilkins, R.G. Compton, Carbon nanotubes contain metal impurities which are responsible for the "electrocatalysis" seen at some nanotube-modified electrodes, Angew. Chem, 45 (2006) 2533-2537. https://doi.org/10.1002/anie.200600033.

[11] H.X. Luo, Z.J. Shi, N.Q. Li, Z.N. Gu, Q.K. Zhuang, Investigation of the electrochemical and electrocatalytic behavior of single-wall carbon nanotube film on a glassy carbon electrode, Anal. Chem., 73 (2001) 915-920. https://doi.org/10.1021/ac000967l.

[12] D. Paolucci, M. Marcaccio, C. Bruno, F. Paolucci, N. Tagmatarchis, M. Prato, Voltammetric quantum charging capacitance behaviour of functionalised carbon nanotubes in solution, Electrochim. Acta, 53 (2008) 4059-4064. https://doi.org/10.1016/j.electacta.2007.10.007.

[13] J.P. Metters, M. Gomez-Mingot, J. Iniesta, R.O. Kadara, C.E. Banks, The fabrication of novel screen printed single-walled carbon nanotube electrodes: Electroanalytical applications, Sensor Actuat. B-Chem., 177 (2013) 1043-1052. https://doi.org/10.1016/j.snb.2012.11.078.

[14] Y.Y. Chan, A.Y.S. Eng, M. Pumera, R.D. Webster, Assessments of surface coverage after nanomaterials are drop cast onto electrodes for electroanalytical applications, ChemElectroChem, 2 (2015) 1003-1009. https://doi.org/10.1002/celc.201500047.

[15] Y.W. Fan, B.R. Goldsmith, P.G. Collins, Identifying and counting point defects in carbon nanotubes, Nat. Mater., 4 (2005) 906-911. DOI: 10.1038/nmat1516.

[16] P. Bertoncello, J.P. Edgeworth, J.V. Macpherson, P.R. Unwin, Trace level cyclic voltammetry facilitated by single-walled carbon nanotube network electrodes, J. Am. Chem. Soc., 129 (2007) 10982-10983. DOI:10.1021/ja073360w.

[17] S.P. E, T.S. Miller, J.V. Macpherson, P.R. Unwin, Controlled functionalisation of single-walled carbon nanotube network electrodes for the enhanced voltammetric detection of dopamine, Phys. Chem. Chem. Phys., 17 (2015) 26394-26402. https://doi.org/10.1039/C5CP04905A.

[18] I. Dumitrescu, J.P. Edgeworth, P.R. Unwin, J.V. Macpherson, Ultrathin carbon nanotube mat electrodes for enhanced amperometric detection, Adv. Mater., 21 (2009) 3105-3109. https://doi.org/10.1002/adma.200900402.

[19] D.M. Pearce, D.P. Shenton, J. Holden, C.A. Gaydos, Evaluation of a novel electrochemical detection method for chlamydia trachomatis: application for point-of-care diagnostics, IEEE T. Bio-Med. Eng., 58 (2011) 755-758. https://doi.org/10.1109/TBME.2010.2095851.

[20] F.A. Larik, A. Saeed, T.A. Fattah, U. Muqadar, P.A. Channar, Recent advances in the synthesis, biological activities and various applications of ferrocene derivatives, Appl. Organomet. Chem., 31 (2017) e3664. https://doi.org/10.1002/aoc.3664.

[21] C.J. Yu, H. Yowanto, Y.J. Wan, T.J. Meade, Y. Chong, M. Strong, L.H. Donilon, J.F. Kayyem, M. Gozin, G.F. Blackburn, uridine-conjugated ferrocene DNA oligonucleotides: Unexpected cyclization reaction of the uridine base, J. Am. Chem. Soc., 122 (2000) 6767-6768. https://doi.org/10.1021/ja994241m.

[22] S.C. Hillier, C.G. Frost, A.T.A. Jenkins, H.T. Braven, R.W. Keay, S.E. Flower, J.M. Clarkson, An electrochemical study of enzymatic oligonucleotide digestion, Bioelectrochemistry, 63 (2004) 307-310. https://doi.org/10.1016/j.bioelechem.2003.10.028.

[23] J. Wang, J.H. Li, A.J. Baca, J.B. Hu, F.M. Zhou, W. Yan, D.W. Pang, Amplified voltammetric detection of DNA hybridization via oxidation of ferrocene caps on gold nanoparticle/streptavidin conjugates, Anal. Chem., 75 (2003) 3941-3945. https://doi.org/10.1021/ac0344079.

[24] J. Wang, X. Yi, H. Tang, H. Han, M. Wu, F. Zhou, Direct quantification of microRNA at low picomolar level in sera of glioma patients using a competitive hybridization followed by amplified voltammetric detection, Anal. Chem., 84 (2012) 6400-6406. https://doi.org/10.1021/ac203368h.

[25] P.H. Lepage, R. Peytavi, M.G. Bergeron, M. Leclerc, Amplification strategy using aggregates of ferrocene-containing cationic polythiophene for sensitive and specific electrochemical detection of DNA, Anal. Chem., 83 (2011) 8086-8092. https://doi.org/10.1021/ac200713f.

[26] J. Wang, Electrochemical glucose biosensors, Chem. Rev., 108 (2008) 814-825. https://doi.org/10.1021/cr068123a.

[27] A.A. D'souza, R. Shegokar, Polyethylene glycol (PEG): a versatile polymer for pharmaceutical applications, Expert Opin. Drug Deliv., 13 (2016) 1257-1275. DOI: 10.1080/17425247.2016.1182485.

[28] J. Li, J. Macdonald, F. von Stetten, Review: a comprehensive summary of a decade development of the recombinase polymerase amplification, Analyst, 144 (2019) 31-67. https://doi.org/10.1039/C8AN01621F.

[29] C. Jiang, G. Wang, R. Hein, N. Liu, X. Luo, J.J. Davis, Antifouling strategies for selective in vitro and in vivo Sensing, Chem. Rev., (2020). https://doi.org/10.1021/acs.chemrev.9b00739.

[30] E. Bahena, P.F. Méndez, Y. Meas, R. Ortega, L. Salgado, G. Trejo, An EQCM study of polyethyleneglycol 8000 adsorption and its coadsorption with Cl− ions on Pt in perchloric acid solutions, Electrochim. Acta, 49 (2004) 989-997. https://doi.org/10.1016/j.electacta.2003.10.010.

[31] L.-H. Li, S. Yau, W.-P. Dow, In situ STM imaging of polyethylene glycol adsorbed on an Au(111) electrode in pH3, Electrochem. commun., 70 (2016) 1-4. https://doi.org/10.1016/j.elecom.2016.06.007.

[32] A.M. Merlot, D.S. Kalinowski, D.R. Richardson, Unraveling the mysteries of serum albumin—more than just a serum protein, Front. Physiol., 5 (2014). https://doi.org/10.3389/fphys.2014.00299.

[33] A.J. Downard, A.D. Roddick, Effect of electrochemical pretreatment on protein adsorption at glassy-carbon electrodes, Electroanalysis, 6 (1994) 409-414. https://doi.org/10.1002/elan.1140060509.

[34] Q. Xie, C. Xiang, Y. Yuan, Y. Zhang, L. Nie, S. Yao, A novel dual-impedance-analysis EQCM system—investigation of bovine serum albumin adsorption on gold and platinum electrode surfaces, J. Colloid Interf. Sci., 262 (2003) 107-115. https://doi.org/10.1016/S0021-9797(03)00196-6.

[35] P.V. Dudin, P.R. Unwin, J.V. Macpherson, Electro-oxidation of hydrazine at gold nanoparticle functionalised single walled carbon nanotube network ultramicroelectrodes, Phys. Chem. Chem. Phys., 13 (2011) 17146-17152. https://doi.org/10.1039/C1CP21937E.

[36] R. Saito, G. Dresselhaus, M.S. Dresselhaus, Physical Properties of Carbon Nanotubes, Imperial College Press, London, 1998.

[37] A.F. Holloway, K. Toghill, G.G. Wildgoose, R.G. Compton, M.A.H. Ward, G. Tobias, S.A. Llewellyn, B. Ballesteros, M.L.H. Green, A. Crossley, Electrochemical opening of single-walled carbon nanotubes filled with metal halides and with closed ends, J. Phys. Chem. C, 112 (2008) 10389-10397. https://doi.org/10.1021/jp802127p.

[38] M.S. Dresselhaus, G. Dresselhaus, R. Saito, A. Jorio, Raman spectroscopy of carbon nanotubes, Phys. Rep., 409 (2005) 47-99. https://doi.org/10.1016/j.physrep.2004.10.006.

[39] M.S. Dresselhaus, G. Dresselhaus, A. Jorio, A.G. Souza, R. Saito, Raman spectroscopy on isolated single wall carbon nanotubes, Carbon, 40 (2002) 2043-2061. https://doi.org/10.1016/S0008-6223(02)00066-0.

[40] V. Skakalova, A.B. Kaiser, W.U. Dettlaff, K. Hrncarikova, S. Roth, Effect of chemical treatment on electrical conductivity, infrared absorption, and Raman spectra of single-walled carbon nanotubes, J. Phys. Chem. B, 109 (2005) 7174-7181. https://doi.org/10.1021/jp044741o.

[41] A. Jorio, R. Saito, G. Dresselhaus, M.S. Dresselhaus, Determination of nanotubes properties by Raman spectroscopy, Philos. T. Roy. Soc. A, 362 (2004) 2311-2336. DOI: 10.1098/rsta.2004.1443.

[42] S.C. Wang, K.S. Chang, C.J. Yuan, Enhancement of electrochemical properties of screen-printed carbon electrodes by oxygen plasma treatment, Electrochim. Acta, 54 (2009) 4937-4943. https://doi.org/10.1016/j.electacta.2009.04.006.

[43] A. Jorio, A.G. Souza, G. Dresselhaus, M.S. Dresselhaus, R. Saito, J.H. Hafner, C.M. Lieber, F.M. Matinaga, M.S.S. Dantas, M.A. Pimenta, Joint density of electronic states for one isolated single-wall carbon nanotube studied by resonant Raman scattering, Phys. Rev. B, 63 (2001) 245416 (1-4). https://doi.org/10.1103/PhysRevB.63.245416

[44] G. Zhang, A.S. Cuharuc, A.G. Güell, P.R. Unwin, Electrochemistry at highly oriented pyrolytic graphite (HOPG): lower limit for the kinetics of outer-sphere redox processes and general implications for electron transfer models, Phys. Chem. Chem. Phys., 17 (2015) 11827-11838. https://doi.org/10.1039/C5CP00383K.

[45] I. Dumitrescu, P.V. Dudin, J.P. Edgeworth, J.V. Macpherson, P.R. Unwin, Electron transfer kinetics at single-walled carbon nanotube electrodes using scanning electrochemical microscopy, J. Phys. Chem. C, 114 (2010) 2633-2639. https://doi.org/10.1021/jp908830d.

[46] W.F. Sokol, D.H. Evans, Suppression of background current in differential pulse voltammetry with solid electrodes, Anal. Chem., 53 (1981) 578-580. https://doi.org/10.1021/ac00227a004.

[47] S.J. Cobb, J.V. Macpherson, Enhancing square wave voltammetry measurements via electrochemical analysis of the non-faradaic potential window, Anal. Chem., 91 (2019) 7935-7942. https://doi.org/10.1021/acs.analchem.9b01857

[48] I. Dumitrescu, P.R. Unwin, J.V. Macpherson, Electrochemical impedance spectroscopy at single-walled carbon nanotube network ultramicroelectrodes, Electrochem. Commun., 11 (2009) 2081-2084. https://doi.org/10.1016/j.elecom.2009.08.057.

[49] R.C. Alkire, P.N. Bartlett, J. Lipkowski, Electrochemistry of Carbon Electrodes, Wiley, 2015.

[50] C.E. Hotchen, I.J. Maybury, G.W. Nelson, J.S. Foord, P. Holdway, F. Marken, Amplified electron transfer at poly-ethylene-glycol (PEG) grafted electrodes, Phys. Chem. Chem. Phys., 17 (2015) 11260-11268. https://doi.org/10.1039/C5CP01244A.

[51] E. Celik, L. Liu, H. Choi, Protein fouling behavior of carbon nanotube/polyethersulfone composite membranes during water filtration, Water Res., 45 (2011) 5287-5294. https://doi.org/10.1016/j.watres.2011.07.036.